Robotica (2022), **40**, pp. 3499–3513
doi:10.1017/S0263574722000376

CAMBRIDGE UNIVERSITY PRESS

RESEARCH ARTICLE

Study on the design and control method of a wire-driven waist rehabilitation training parallel robot

Wang Yuqi[1], Cao Jinjiang[1], Geng Ranran[2], Zhou Lei[1] and Wang Lei[1]

[1]School of Automation, Nanjing Institute of Technology, Nanjing, China and [2]Industrial Center, Nanjing Institute of Technology, Nanjing, China
Corresponding author. E-mail: 940898628@qq.com

Received: 17 June 2021; **Revised:** 21 January 2022; **Accepted:** 24 February 2022; **First published online:** 28 March 2022

Keywords: wire-driven rehabilitation training robot, prototype design, modeling analysis, intelligent control, simulation analysis

Abstract

With the increasing demand for rehabilitation and the lack of professional rehabilitation personnel, robot-assisted rehabilitation technology plays an increasingly important role in neurological rehabilitation. In order to recover the exercise ability of patients with waist injury, a new type of wire-driven waist rehabilitation training parallel robot (WWRTPR) is designed. According to the motion trajectory planning of waist rehabilitation training, two coordinate systems are established: moving coordinate system and static coordinate system. The inverse kinematics modeling analysis is carried out, and the dynamic model of the robot is established by using Newton–Euler method. An intelligent control method of force/position hybrid control based on radial basis function neural network is proposed. The stability of the closed-loop system is analyzed, and the results show that WWRTPR tends to be stable. The simulation analysis of rehabilitation training on WWRTPR is carried out, and the simulation results show that the proposed intelligent control method can effectively control the robot system, which provides a reference for the development of a flexible intelligent rehabilitation training robot.

1. Introduction

With the increase of stroke, disability and dementia, the number of patients with limb dysfunction are also increasing. In order to recover the patients' life and labour ability to the maximum extent, rehabilitation training robot is one of the most active and effective ways. The traditional rehabilitation training robot mostly uses rigid connecting rod and other mechanisms to realize the transmission, which is very complicated when performing multi-degree-of-freedom control and the mechanical structure has a large mass. At the same time, the rigid connecting rod mechanism is insufficient in the adjustment and adaptability of patients with different body types, and the flexibility of the physical system is relatively poor. It may even cause wrong movements in rehabilitation training and bring secondary injuries to patients.

In order to improve the cooperative relationship between the robot and the patient, in view of the deficiencies of rigid linkages and other mechanisms, and considering the safety, comfort and flexibility of patients, the combination of the wire-driven parallel robot technology and rehabilitation training technology has opened up a new idea for the development and innovation of rehabilitation training robot. Compared with the rigid parallel robot, the wire-driven parallel robot has a series of advantages, such as simple structure, large workspace, good dynamic performance and high degree of modularization [1, 2]. As a product of the combination of robot technology and medical technology, the wire-driven rehabilitation training parallel robot is a highly intersecting robot which integrates robotics, biomedicine, artificial intelligence and other disciplines. It performs repetitive training based on the principle of neural plasticity. The training positions (waist, upper limb, lower limb, etc.) are different according to the needs of patients [3, 4, 5, 6]. It is the frontier technical approach to solve the problem of patient rehabilitation training.

At present, experts and scholars from domestic and foreign organizations have carried out relevant research on the wire-driven rehabilitation training parallel robot and its control technology. Soheil et al. [7] proposed a computational torque control algorithm for a four-wire driven parallel robot used for gait rehabilitation training, and the tracking error was reduced by using PD controller. Hamed et al. proposed a controller based on AAN advantages of model and non-model for a new four-wire driven planar robot, which improved the efficiency of rehabilitation training. The effectiveness of the proposed control scheme was verified by gait rehabilitation simulation [8]. Yupeng et al. [9] proposed an active force control strategy for a mobile cable-driven lower limb rehabilitation training robot, and verified through experiments that the proposed control strategy could significantly improve the loading accuracy and dynamic performance of the servo system. Gabriel et al. designed and developed a portable cable-driven exoskeleton robot, and proposed an exoskeleton control for rehabilitation training. At the same time, the effectiveness of the proposed torque control strategy is verified through experiments [10]. Rong et al. [11] proposed a performance-based hybrid control method for a cable-driven upper limb rehabilitation training robot and verified the effectiveness of the controller through experiments. Jarrett et al. [12] proposed a sliding mode controller to realize low-order torque control for a new type of cable-driven soft joint, and verified the robustness of the proposed control strategy through experiments. Chen et al. designed and developed a new type of cable-driven lumbar rehabilitation training parallel robot, which adopted a two-stage control algorithm to assist the patients with lumbar injury in rehabilitation training. The experimental results show that the designed control algorithm can improve the performance of the system [13].

Through the above research and analysis, it can be concluded that the research on the wire-driven rehabilitation training parallel robot is mainly based on upper limbs robots, lower limbs robots and the exoskeleton robots of lower limbs, especially the research on the exoskeleton rehabilitation training robot of lower limbs. But the research on the wire-driven rehabilitation training parallel robot for patients with lumbar injury is relatively less. Therefore, based on the technology theory of the wire-driven parallel robot and combined with the characteristics of rehabilitation training for patients with lumbar injury, a new type of wire-driven lumbar rehabilitation training parallel robot is designed. The contribution and innovation of this article are that the lumbar rehabilitation training parallel robot is designed based on the wire system time-varying structure and a new hybrid force/position intelligent control method based on radial basis function (RBF) neural network is proposed in order to achieve the purpose of rehabilitation training. And the motion performance of the robot and the effectiveness of the proposed control method are verified by simulation analysis.

The rest of this study is organized as follows. In Section 2, the design of the prototype system is described. Sections 3 and 4 present kinematics model and dynamic model of the wire-driven waist rehabilitation training parallel robot (WWRTPR), respectively. Moreover, the design of the control law and Lyapunov stability analysis are addressed in Section 5. In Section 6, simulation analysis and results are given. Finally, Section 7 concludes the paper.

2. Design of prototype system

Three-dimensional six-degree-of-freedom motion of human lumbar spine—three-dimensional refers to three motion axes (coronal axis, sagittal axis, vertical axis), six-degree-of-freedom motion refers to three angular displacements and three linear displacements. This paper is mainly to achieve the lumbar rehabilitation training of patients through the wire-driven moving platform. As shown in Fig. 1, it is a three-dimensional model of the wire-driven lumbar rehabilitation training parallel robot.

In this paper, the wire-driven lumbar rehabilitation training parallel robot is mainly composed of brace, wire-driven moving platform, wire-driven system, control system, weight reduction system, lower limb fixed adjustment device, universal pulley, lifting platform, etc., to realize the rehabilitation training of patients with three-dimensional six-degree-of-freedom movement.

The brace is made of 1.5 and 2 m square aluminum profiles, respectively. The wire-driven system is mainly composed of four groups of servo motors, ball screw and moving slider, etc., which are used

https://doi.org/10.1017/S0263574722000376 Published online by Cambridge University Press

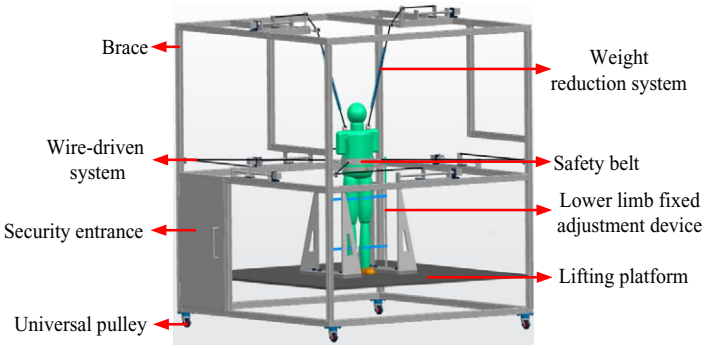

Figure 1. *3D model of WWRTPR.*

to drive four wires, so as to change the length and direction of the wire through the pulley. The weight reduction system is mainly composed of two groups of servo motor, ball screw, fixed pulley, weight reduction spring, load-bearing vest, etc. the wire is driven by the servo motor, so as to stretch the spring to generate tension on the human body and achieve the purpose of weight reduction during rehabilitation training. The lower limb fixed adjustment device is fixed on the lifting platform, which is mainly composed of thigh adjustment module and calf adjustment module. The belt of thigh and calf is adjusted according to the patient's weight, and the rise and fall of the lifting platform are adjusted according to the patient's height, so as to ensure the safety and comfort of patients in rehabilitation training. The designed wire-driven rehabilitation training parallel robot can provide different contact forces to meet the use requirements of different patients according to the needs of patients [14].

3. Kinematics modeling analysis

In the rehabilitation training operation of WWRTPR, the motion trajectory planning of rehabilitation training is essentially an inverse kinematics problem. The inverse kinematics modeling is established according to the relationship between the wire length and the pose of the end effector (patient), that is, the variation of the wire length causes the adjustment of the patient's pose. The kinematic model of the system is established to lay a theoretical foundation for the dynamic modeling. The structural schematic diagram of WWRTPR is shown in Fig. 2.

In Fig. 2, the static coordinate system (OXYZ) is fixed on the lifting platform and the moving coordinate system (PXYZ) is established at the waist of the patient, and the initial direction of the coordinate axes of the two coordinate systems is the same. Four traction wires (wire 1, wire 2, wire 3, wire 4) are used to drive patients to achieve spatial movement of six-degree-of-freedom, and the movement of the four traction wires is independent of each other. Two traction wires (O_1I_1, O_2I_2) and springs are used for weight reduction.

The kinematic diagram of the system is shown in Fig. 3. Where, set $\boldsymbol{P}_i = \overline{\overline{OP_i}}$, $\boldsymbol{B}_i = \overline{\overline{OB_i}}$, in the static coordinate system, the wire length vector $\boldsymbol{L}_i$ satisfies

$$\boldsymbol{L}_i = \boldsymbol{X}_P + \boldsymbol{R}\boldsymbol{x}_{P_i} - \boldsymbol{B}_i \tag{1}$$

where $\boldsymbol{X}_P(X_P, Y_P, Z_P)^{\mathrm{T}}$ is the coordinate of the origin P of the moving coordinate system in the static coordinate system; $\boldsymbol{C}_0(x_{P_i}, y_{P_i}, z_{P_i})^{\mathrm{T}}$ is the coordinate of P_i in the moving coordinate system Pxyz ($i = 1,\ldots,4$, i is the value of the wire); $\boldsymbol{R}$ is the rotation transformation matrix from the moving coordinate system to the static coordinate system, which can be expressed as

$$\boldsymbol{R} = \begin{bmatrix} c\theta c\psi & s\phi s\theta c\psi - c\phi s\psi & c\phi s\theta c\psi + s\phi s\psi \\ c\theta s\psi & s\phi s\theta s\psi + c\phi c\psi & c\phi s\theta s\psi - s\phi c\psi \\ -s\theta & s\phi c\theta & c\phi c\theta \end{bmatrix} \tag{2}$$

https://doi.org/10.1017/S0263574722000376 Published online by Cambridge University Press

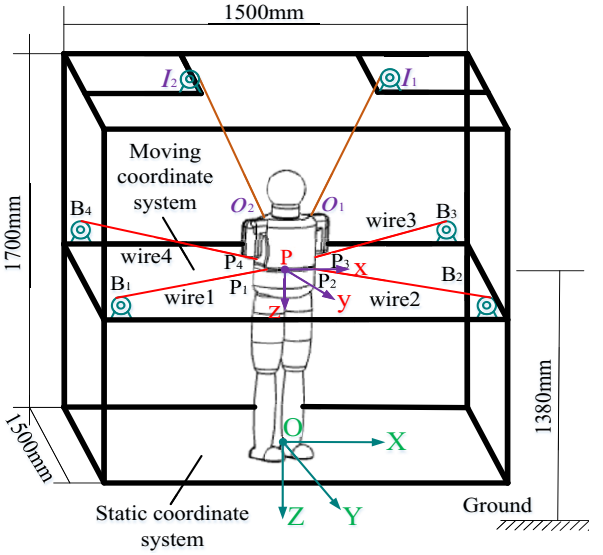

Figure 2. *Structural schematic diagram of WWRTPR.*

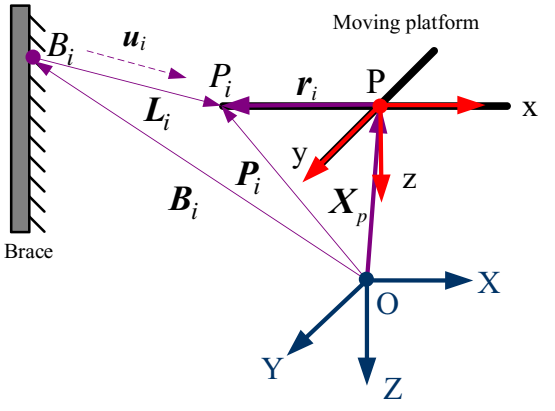

Figure 3. *Kinematic diagram of WWRTPR.*

where ϕ, θ, ψ, respectively, represent the forward and backward swing angle, left and right swing angle and roll angle of the patient's waist rotating around the OX axis, OY axis and OZ axis in the static coordinate system (OXYZ).

Set the length of the ith wire as L_i $(i = 1, \ldots, 4)$, and its expression is

$$L_i = \sqrt{\left(\boldsymbol{X}_P + \boldsymbol{R}\boldsymbol{x}_{P_i} - \boldsymbol{B}_i\right)^{\mathrm{T}}\left(\boldsymbol{X}_P + \boldsymbol{R}\boldsymbol{x}_{P_i} - \boldsymbol{B}_i\right)} \tag{3}$$

where $\boldsymbol{B}_i(X_{B_i}, Y_{B_i}, Z_{B_i})^{\mathrm{T}}$ is the coordinate of each hinge point B_i in the static coordinate system.

The time derivative of the rotation transformation matrix $\boldsymbol{R}$ can be obtained as follows:

$$\dot{\boldsymbol{R}} = \boldsymbol{R}^{\mathrm{o}}\boldsymbol{R} \tag{4}$$

where $\boldsymbol{R}^{\mathrm{o}} = \begin{bmatrix} 0 & -\omega_Z & \omega_Y \\ \omega_Z & 0 & -\omega_X \\ -\omega_Y & \omega_X & 0 \end{bmatrix}$, $\boldsymbol{\omega}$ is the angular velocity, $\boldsymbol{R}^{\mathrm{o}} = \boldsymbol{\omega}^{\times}$, ($\boldsymbol{\omega}^{\times}$ is the antisymmetric matrix of $\boldsymbol{\omega}$).

https://doi.org/10.1017/S0263574722000376 Published online by Cambridge University Press

By substituting Eq. (4) into Eq. (3) and simplifying, the following results can be obtained:

$$L_i\dot{L}_i = (\boldsymbol{L}_i)^{\mathrm{T}}\left(\dot{\boldsymbol{X}}_P + \boldsymbol{R}^{\mathrm{o}}\boldsymbol{R}\boldsymbol{x}_{P_i}\right) \tag{5}$$

Let $\boldsymbol{r}_i = \boldsymbol{R}\boldsymbol{x}_{P_i}$, then,

$$L_i\dot{L}_i = (\boldsymbol{L}_i)^{\mathrm{T}}\,\dot{\boldsymbol{X}}_P + (\boldsymbol{L}_i)^{\mathrm{T}}\left(\boldsymbol{\omega}^{\times}\boldsymbol{r}_i\right) \tag{6}$$

Since $\dot{\boldsymbol{r}}_i = \boldsymbol{R}^{\mathrm{o}}\boldsymbol{R}\boldsymbol{x}_{P_i}, \boldsymbol{R}^{\mathrm{o}} = \boldsymbol{\omega}^{\times}$, then $\dot{\boldsymbol{r}}_i = \boldsymbol{\omega}^{\times}\boldsymbol{r}_i$. Through the example of MATLAB, it is proved that:

$$\boldsymbol{\omega}^{\times}\boldsymbol{r}_i = -\boldsymbol{r}_i{}^{\times}\boldsymbol{\omega},\ \boldsymbol{\omega}^{\times}\boldsymbol{r}_i = \boldsymbol{\omega}\times\boldsymbol{r}_i \tag{7}$$

Therefore,

$$L_i\dot{L}_i = (\boldsymbol{L}_i)^{\mathrm{T}}\,\dot{\boldsymbol{X}}_P + (\boldsymbol{L}_i)^{\mathrm{T}}(\boldsymbol{\omega}\times\boldsymbol{r}_i) \tag{8}$$

Through sorting out Eq. (8), it can be concluded that:

$$L_i\dot{L}_i = (\boldsymbol{L}_i)^{\mathrm{T}}\,\dot{\boldsymbol{X}}_P + (\boldsymbol{r}_i\times\boldsymbol{L}_i)^{\mathrm{T}}\,\boldsymbol{\omega} \tag{9}$$

When Eq. (9) is written in the form of matrix, it can be obtained:

$$\tilde{\boldsymbol{L}}\dot{\boldsymbol{L}} = \tilde{\boldsymbol{J}}_A\dot{\boldsymbol{X}}_\omega \tag{10}$$

The matrices in Eq. (10) are successively defined as

$$\dot{\boldsymbol{X}}_\omega = \begin{bmatrix}\dot{\boldsymbol{X}}_P\\ \boldsymbol{\omega}\end{bmatrix} = \begin{bmatrix}\boldsymbol{v}\\ \boldsymbol{\omega}\end{bmatrix} = \boldsymbol{G}\dot{\boldsymbol{X}},\ \dot{\boldsymbol{L}} = \begin{bmatrix}\dot{L}_1 & \dot{L}_2 & \dot{L}_3 & \dot{L}_4\end{bmatrix}^{\mathrm{T}} = \boldsymbol{J}\boldsymbol{G}\dot{\boldsymbol{X}},\ \tilde{\boldsymbol{L}} = \mathrm{diag}\begin{bmatrix}L_1 & L_2 & L_3 & L_4\end{bmatrix},$$

$$\tilde{\boldsymbol{J}}_A^{\mathrm{T}} = \begin{bmatrix}\boldsymbol{L}_1 & \boldsymbol{L}_2 & \boldsymbol{L}_3 & \boldsymbol{L}_4\\ \boldsymbol{r}_1\times\boldsymbol{L}_1 & \boldsymbol{r}_2\times\boldsymbol{L}_2 & \boldsymbol{r}_3\times\boldsymbol{L}_3 & \boldsymbol{r}_4\times\boldsymbol{L}_4\end{bmatrix}.$$

where $\dot{\boldsymbol{X}}_\omega$ is the motion velocity vector of the patient model, which includes the linear velocity $\boldsymbol{v}$ and angular velocity $\boldsymbol{\omega}$ of the patient model relative to the brace, $\boldsymbol{J}$ is the Jacobian matrix of 4×6, $\boldsymbol{G}$ is the transformation matrix based on attitude angle, and $\boldsymbol{G} = \begin{bmatrix}\boldsymbol{I}_{3\times3} & \boldsymbol{0}_{3\times3}\\ \boldsymbol{0}_{3\times3} & \boldsymbol{H}\end{bmatrix}, \boldsymbol{H} = \begin{bmatrix}\mathrm{c}\theta\mathrm{c}\psi & -\mathrm{s}\psi & 0\\ \mathrm{c}\theta\mathrm{s}\psi & \mathrm{c}\psi & 0\\ -\mathrm{s}\theta & 0 & 1\end{bmatrix}$.

4. Dynamic modeling analysis

The purpose of building dynamic model is to study the relationship between the mechanism motion and the force of WWRTPR. The main purpose of the research is to design the motion control, so as to realize the specific motion of the end effector (patient) of the parallel robot and achieve the optimal control goal or better dynamic performance.

The dynamic model of WWRTPR includes three parts: dynamic model of moving platform, elastic dynamic model of wire and dynamic model of driving system, and the dynamic model of the moving platform (the end effector) is the basis of motion control design. The dynamic symbol schematic diagram of defining the system is shown in Fig. 4.

Since the mass of the wire is much smaller than the sum of the mass and load of the end effector (the patient's moving platform), the mass and inertia of the driving wire are ignored, and the elastic model of the wire is not considered, so as to simplify the dynamic model of the system. The dynamic model of the whole system is composed of the dynamic model of the patient's moving platform and the dynamic model of the driving system. The two dynamic models are combined to obtain the dynamic model of the whole system.

The Newton–Euler method is used to establish the dynamic equation of the wire-driven lumbar rehabilitation training parallel robot relative to the origin P of the moving coordinate system, the established

https://doi.org/10.1017/S0263574722000376 Published online by Cambridge University Press

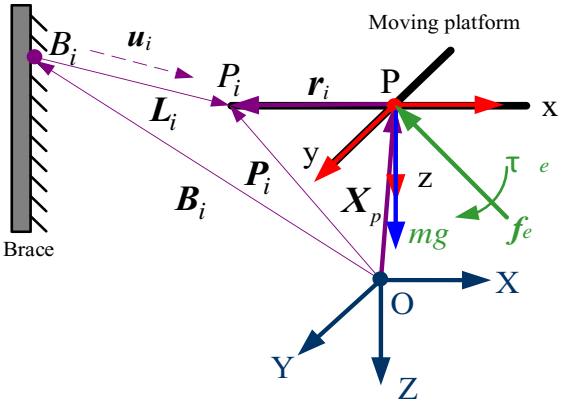

Figure 4. *Dynamic diagram of WWRTPR.*

dynamic equation is as follows:

$$\begin{cases} m\ddot{\boldsymbol{P}} = \boldsymbol{f}_e + \sum_{i=1}^{4} (-T_i \boldsymbol{u}_i) + m\boldsymbol{g} \\ \boldsymbol{A}_G \dot{\boldsymbol{\omega}} = \boldsymbol{\tau}_e + \sum_{i=1}^{4} \boldsymbol{r}_i \times (-T_i \boldsymbol{u}_i) - \boldsymbol{\omega} \times (\boldsymbol{A}_G \boldsymbol{\omega}) \end{cases} \tag{11}$$

where m is the mass of the end effector (patient), $\ddot{\boldsymbol{P}} = \left(\ddot{X}_P, \ddot{Y}_P, \ddot{Z}_P\right)^{\mathrm{T}}$ is the linear acceleration vector of the reference point p of the end effector, $\boldsymbol{f}_e$ and $\boldsymbol{\tau}_e$ are, respectively, the external forces and torques acting on the patient, $\boldsymbol{u}_i = \frac{\boldsymbol{L}_i}{L_i}$ is the tension vector of the wire, T_i is the tension of the ith wire, and $\boldsymbol{g}$ is the gravity acceleration vector, $\boldsymbol{A}_G^*$ is the inertia matrix of the end effector with respect to the center of gravity, $\boldsymbol{A}_G = \boldsymbol{R}\boldsymbol{A}_G^*\boldsymbol{R}^{\mathrm{T}}$ and $\dot{\boldsymbol{\omega}}$ is the angular acceleration vector.

According to the dynamic torque balance equation, the dynamic equation of the driving system is as follows:

$$\boldsymbol{M}_0 \ddot{\boldsymbol{\theta}}_m + \boldsymbol{C}_0 \dot{\boldsymbol{\theta}}_m + \boldsymbol{\tau}_l = \boldsymbol{\tau} \tag{12}$$

where $\boldsymbol{M}_0$ is the inertia matrix equivalent to the actuator; $\boldsymbol{C}_0$ is the viscous friction coefficient matrix equivalent to the actuator; $\boldsymbol{\theta}_m$ is the motor rotation angle; $\boldsymbol{\tau}_l = \mu \boldsymbol{u}$ is the load moment generated by the wire tension; $\boldsymbol{\tau}$ is the output torque vector of the driver.

The generalized force acting on the system is $\boldsymbol{F} = \begin{bmatrix} F_x & F_y & F_z & M_x & M_y & M_z \end{bmatrix}$, then $\boldsymbol{F}$ has the following relationship with the matrix and the tension of the wire:

$$\boldsymbol{u} = (\boldsymbol{J}^{\mathrm{T}})^{+} \boldsymbol{F} \tag{13}$$

where $\boldsymbol{u} = [u_1 \quad u_2 \quad u_3 \quad u_4]^{\mathrm{T}}$ is the tension vector of four wires, and $(\boldsymbol{J}^{\mathrm{T}})^{+}$ is the pseudo inverse matrix of $\boldsymbol{J}^{\mathrm{T}}$ [15, 16].

Equations (11) and (12), as well as the relationship among wire length $\boldsymbol{L}$, motor rotation angle $\boldsymbol{\theta}_m$ and patient posture $\boldsymbol{X}$, are used to construct the whole dynamic equation of the system (as shown in Eq. (14)), which lays a theoretical foundation for the subsequent studies.

$$\begin{aligned} &\left(\boldsymbol{M}(\boldsymbol{X}) - \frac{1}{\mu^2} \cdot \boldsymbol{J}^{\mathrm{T}} \boldsymbol{M}_0 \boldsymbol{J} \boldsymbol{G}\right) \ddot{\boldsymbol{X}} - \frac{1}{\mu^2} \left(\boldsymbol{J}^{\mathrm{T}} \boldsymbol{M}_0 \dot{\boldsymbol{J}} \boldsymbol{G} + \boldsymbol{J}^{\mathrm{T}} \boldsymbol{M}_0 \boldsymbol{J} \dot{\boldsymbol{G}} + \boldsymbol{J}^{\mathrm{T}} \boldsymbol{C}_0 \boldsymbol{J} \boldsymbol{G}\right) \dot{\boldsymbol{X}} \\ &= -\frac{1}{\mu} \cdot \boldsymbol{J}^{\mathrm{T}} \boldsymbol{\tau} + \boldsymbol{w}_g + \boldsymbol{w}_e - \boldsymbol{N}\left(\boldsymbol{X}, \dot{\boldsymbol{X}}\right) \end{aligned} \tag{14}$$

where $\boldsymbol{M}(\boldsymbol{X})$ is the inertia matrix of the end effector (patient), $\boldsymbol{X}$ is the actual pose of the end effector (patient), μ is the transmission coefficient, $\boldsymbol{J}$ is the Jacobian matrix of the system, $\boldsymbol{w}_g$ is the gravity vector of the end effector, $\boldsymbol{w}_e = [f_e; \tau_e]$, and $\boldsymbol{N}\left(\boldsymbol{X}, \dot{\boldsymbol{X}}\right)$ is the nonlinear Coriolis centrifugal force matrix.

https://doi.org/10.1017/S0263574722000376 Published online by Cambridge University Press

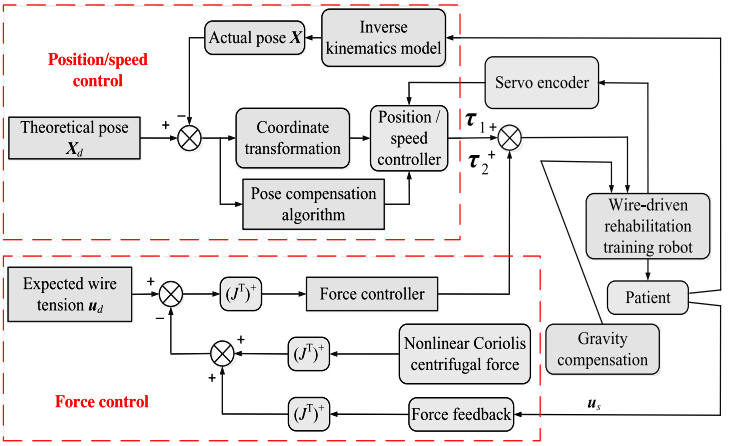

Figure 5. *Structure schematic diagram of force/position hybrid control of WWRTPR.*

5. Control law design and stability analysis

The research object of this article, the WWRTPR, is a complex strong coupling, multi-input and multi-output, and nonlinear time-varying system, which has strict requirements for flexibility, safety and comfort. Therefore, the design of its motion control strategy (considering force and pose) is extremely important.

5.1. Design of control law

The ideal motion trajectory of waist rehabilitation training is set as $\boldsymbol{X}_d$, the motion tracking error is defined as $\boldsymbol{e} = \boldsymbol{X} - \boldsymbol{X}_d$, the velocity error is defined as $\dot{\boldsymbol{e}} = \dot{\boldsymbol{X}} - \dot{\boldsymbol{X}}_d$ and the acceleration error is defined as $\ddot{\boldsymbol{e}} = \ddot{\boldsymbol{X}} - \ddot{\boldsymbol{X}}_d$. In order to improve the motion control accuracy of patients and the control performance of the system, referring to the design advantages of literature [17–24] and combining with the rehabilitation training characteristics of WWRTPR, an intelligent control method of force/position hybrid control based on RBF neural network is proposed, as shown in Eq. (15), and the structural schematic diagram of force/position hybrid control is designed, as shown in Fig. 5.

$$\boldsymbol{\tau} = \boldsymbol{\tau}_1 + \boldsymbol{\tau}_2 \tag{15}$$

where $\boldsymbol{\tau}$ is the total control law, $\boldsymbol{\tau}_1$ is the position control law, and $\boldsymbol{\tau}_2$ is the force control law. Among them,

$$\begin{aligned}\boldsymbol{\tau}_1 = -\mu\left(\boldsymbol{J}^{\mathrm{T}}\right)^{+}\left\{\left(\boldsymbol{M}(\boldsymbol{X}) - \frac{1}{\mu^2}\cdot\boldsymbol{J}^{\mathrm{T}}\boldsymbol{M}_0\boldsymbol{J}\boldsymbol{G}\right)\ddot{\boldsymbol{X}}_d + \left[-\frac{1}{\mu^2}\left(\boldsymbol{J}^{\mathrm{T}}\boldsymbol{M}_0\dot{\boldsymbol{J}}\boldsymbol{G} + \boldsymbol{J}^{\mathrm{T}}\boldsymbol{M}_0\boldsymbol{J}\dot{\boldsymbol{G}} + \boldsymbol{J}^{\mathrm{T}}\boldsymbol{C}_0\boldsymbol{J}\boldsymbol{G}\right)\right]\dot{\boldsymbol{X}}_d\right.\\ \left. + \boldsymbol{N}\left(\boldsymbol{X},\dot{\boldsymbol{X}}\right) + \boldsymbol{\lambda} - \boldsymbol{K}_p\boldsymbol{e} - \boldsymbol{K}_d\dot{\boldsymbol{e}}\right\}\end{aligned} \tag{16}$$

Let $\boldsymbol{K}_1 = \boldsymbol{M}(\boldsymbol{X}) - \frac{1}{\mu^2}\cdot\boldsymbol{J}^{\mathrm{T}}\boldsymbol{M}_0\boldsymbol{J}\boldsymbol{G}, \boldsymbol{K}_2 = -\frac{1}{\mu^2}\left(\boldsymbol{J}^{\mathrm{T}}\boldsymbol{M}_0\dot{\boldsymbol{J}}\boldsymbol{G} + \boldsymbol{J}^{\mathrm{T}}\boldsymbol{M}_0\boldsymbol{J}\dot{\boldsymbol{G}} + \boldsymbol{J}^{\mathrm{T}}\boldsymbol{C}_0\boldsymbol{J}\boldsymbol{G}\right), \boldsymbol{K}_3 = \boldsymbol{N}\left(\boldsymbol{X},\dot{\boldsymbol{X}}\right) - \boldsymbol{w}_g - \boldsymbol{w}_e$, then,

$$\boldsymbol{\tau}_1 = -\mu\left(\boldsymbol{J}^{\mathrm{T}}\right)^{+}\left(\boldsymbol{K}_1\ddot{\boldsymbol{X}}_d + \boldsymbol{K}_2\dot{\boldsymbol{X}}_d + \boldsymbol{N}\left(\boldsymbol{X},\dot{\boldsymbol{X}}\right) + \boldsymbol{\lambda} - \boldsymbol{K}_p\boldsymbol{e} - \boldsymbol{K}_d\dot{\boldsymbol{e}}\right) \tag{17}$$

$$\boldsymbol{\tau}_2 = -\mu\left(\boldsymbol{J}^{\mathrm{T}}\right)^{+}\left(\boldsymbol{F}_d - \boldsymbol{F}_s - \boldsymbol{N}\left(\boldsymbol{X},\dot{\boldsymbol{X}}\right)\right) \tag{18}$$

In Eqs. (17) and (18), $\boldsymbol{u}_d = (\boldsymbol{J}^{\mathrm{T}})^{+}\boldsymbol{F}_d$ is the expected wire tension vector, $\boldsymbol{u}_s = (\boldsymbol{J}^{\mathrm{T}})^{+}\boldsymbol{F}_s$ is the actual wire tension vector, $\boldsymbol{e}_F = \boldsymbol{F}_d - \boldsymbol{F}_s$, $\boldsymbol{\lambda}$ is external interference, dynamic coupling and patient diversity, etc., $\boldsymbol{K}_p$ is the proportional gain matrix, and $\boldsymbol{K}_d$ is the differential gain matrix.

https://doi.org/10.1017/S0263574722000376 Published online by Cambridge University Press

By substituting $\boldsymbol{\tau}$ into the whole dynamic equation (14) of the system, the error closed-loop equation of the system can be obtained:

$$\boldsymbol{K}_1\ddot{\boldsymbol{e}} + (\boldsymbol{K}_2 + \boldsymbol{K}_d)\dot{\boldsymbol{e}} + \boldsymbol{K}_p\boldsymbol{e} = \boldsymbol{\lambda} + \boldsymbol{w}_g + \boldsymbol{w}_e - \boldsymbol{e}_F - \boldsymbol{N}\left(\boldsymbol{X}, \dot{\boldsymbol{X}}\right) \tag{19}$$

where $(\boldsymbol{J}^{\mathrm{T}})(\boldsymbol{J}^{\mathrm{T}})^{+} = \boldsymbol{I}_{6\times6}$, $(\boldsymbol{J})^{+}\boldsymbol{J} = \boldsymbol{I}_{6\times6}$.

Let $\boldsymbol{u}_1 = -\boldsymbol{N}\left(\boldsymbol{X}, \dot{\boldsymbol{X}}\right) - \boldsymbol{e}_F$, $\boldsymbol{u}_1$ is the feedback control law; let $\Delta\delta = \boldsymbol{\lambda} + \boldsymbol{w}_g + \boldsymbol{w}_e$, $\Delta\delta$ is the uncertainty and external disturbance of the system, and RBF neural network is used to approximate compensation $\Delta\delta$, the expression is as follows:

$$\Delta\delta = \boldsymbol{W}_f{}^{*}\boldsymbol{h}(\boldsymbol{x}) + \xi_f \tag{20}$$

where ξ_f is the approximation error, $\boldsymbol{W}_f{}^{*}$ is the ideal neural network weight, and $\boldsymbol{h}(\boldsymbol{x})$ is the RBF Gaussian function.

By defining $\boldsymbol{x}_1 = \boldsymbol{e}$ and $\boldsymbol{x}_2 = \dot{\boldsymbol{e}} + \varepsilon\boldsymbol{e}$, Eq. (19) is transformed into:

$$\begin{cases} \dot{\boldsymbol{x}}_1 = \boldsymbol{x}_2 - \varepsilon\boldsymbol{x}_1 \\ \boldsymbol{K}_1\dot{\boldsymbol{x}}_2 = -(\boldsymbol{K}_2 + \boldsymbol{K}_d)\boldsymbol{x}_2 - \boldsymbol{K}_p\boldsymbol{e} + \Delta\delta \\ \qquad\quad + \boldsymbol{u}_1 + (\boldsymbol{K}_2 + \boldsymbol{K}_d)\varepsilon\boldsymbol{e} + \boldsymbol{K}_1\varepsilon\dot{\boldsymbol{e}} \end{cases} \tag{21}$$

where $\varepsilon > 0$.

Based on HJI theorem, Eq. (21) is written in the form of Eq. (22):

$$\begin{cases} \boldsymbol{x} = \boldsymbol{f}(\boldsymbol{x}) + \boldsymbol{g}(\boldsymbol{x})\boldsymbol{\lambda} \\ \boldsymbol{z} = \boldsymbol{l}(\boldsymbol{x}) \end{cases} \tag{22}$$

where $\boldsymbol{f}(\boldsymbol{x}) = \begin{bmatrix} \boldsymbol{x}_2 - \varepsilon\boldsymbol{x}_1 \\ \boldsymbol{K}_1{}^{-1}(-(\boldsymbol{K}_2 + \boldsymbol{K}_d)\boldsymbol{x}_2 - \boldsymbol{K}_p\boldsymbol{e} + W_f{}^{*}h(\boldsymbol{x}) \\ \quad + u_1 + (\boldsymbol{K}_2 + \boldsymbol{K}_d)\varepsilon\boldsymbol{e} + \boldsymbol{K}_1\varepsilon\dot{\boldsymbol{e}}) \end{bmatrix}$, $\boldsymbol{g}(\boldsymbol{x}) = \begin{bmatrix} 0 \\ \boldsymbol{K}_1{}^{-1} \end{bmatrix}$, $\boldsymbol{\lambda} = \xi_f$.

Define the evaluation index $\boldsymbol{z}$: since $\boldsymbol{\lambda} = \xi_f$, that is, the approximation error is considered as external interference ξ_f, and the evaluation index is defined as $\boldsymbol{z} = \boldsymbol{x}_2 = \dot{\boldsymbol{e}} + \varepsilon\boldsymbol{e}$, then L_2 gain is $J = \sup_{||\xi_f||\neq0} \frac{||z||_2}{||\xi_f||_2}$. HJI theorem is for a positive number η, if there is a positive definite and differentiable function $V(x) \geqslant 0$ and $\dot{V}(x) \leqslant \frac{1}{2}\left\{\eta^2 ||\boldsymbol{\lambda}||^2 - ||\boldsymbol{z}||^2\right\}$ $(\forall\boldsymbol{\lambda})$, then $J \leqslant \eta$.

Based on Eq. (21), the following adaptive control law is designed

$$\dot{\hat{\boldsymbol{W}}}_f = \alpha\boldsymbol{x}_2\boldsymbol{h}(\boldsymbol{x})^{\mathrm{T}} \tag{23}$$

where $\alpha > 0$.

The feedback control law is designed as follows:

$$\boldsymbol{u}_1 = -(\boldsymbol{K}_2 + \boldsymbol{K}_d)\varepsilon\boldsymbol{e} - \boldsymbol{K}_1\varepsilon\dot{\boldsymbol{e}} - \frac{1}{2}\boldsymbol{x}_2 + \boldsymbol{K}_p\boldsymbol{e} - \frac{1}{2\eta^2}\boldsymbol{x}_2 - \frac{1}{2}\dot{\boldsymbol{K}}_1\boldsymbol{x}_2 - \hat{\boldsymbol{W}}_f\boldsymbol{h}(\boldsymbol{x}) \tag{24}$$

where $\hat{\boldsymbol{W}}_f$ is the estimated weight of the neural network. Then the closed-loop system, that is, Eq. (19) satisfies $J \leq \eta$.

5.2. Stability analysis

In order to verify the stability of the closed-loop system, based on refs. [25–30], the following Lyapunov function is constructed

$$V = \frac{1}{2}\boldsymbol{x}_2{}^{\mathrm{T}}\boldsymbol{K}_1\boldsymbol{x}_2 + \frac{1}{2\alpha}\left|\left|\boldsymbol{W}_f\right|\right|^2 \tag{25}$$

where $\tilde{\boldsymbol{W}}_f = \hat{\boldsymbol{W}}_f - \boldsymbol{W}_f{}^{*}$, $\alpha > 0$. Since $\boldsymbol{K}_1$ is a positive definite matrix, $V > 0$.

https://doi.org/10.1017/S0263574722000376 Published online by Cambridge University Press

Let $||\boldsymbol{P}||^2 = \mathrm{tr}(\boldsymbol{P}\boldsymbol{P}^{\mathrm{T}}) = \mathrm{tr}(\boldsymbol{P}^{\mathrm{T}}\boldsymbol{P})$, where $\mathrm{tr}(\cdot)$ is the matrix trace, then $\left|\left|\boldsymbol{W}_f\right|\right|^2 = \mathrm{tr}\left(\boldsymbol{W}_f{}^{\mathrm{T}}\boldsymbol{W}_f\right)$.
By deriving V, the following results can be obtained:

$$\begin{aligned}\dot{V} &= \boldsymbol{x}_2{}^{\mathrm{T}}\boldsymbol{K}_1\dot{\boldsymbol{x}}_2 + \frac{1}{2}\boldsymbol{x}_2{}^{\mathrm{T}}\dot{\boldsymbol{K}}_1\boldsymbol{x}_2 + \frac{1}{\alpha}\mathrm{tr}\left(\dot{\tilde{\boldsymbol{W}}}_f{}^{\mathrm{T}}\tilde{\boldsymbol{W}}_f\right)\\ &= \boldsymbol{x}_2{}^{\mathrm{T}}\left(-\left(\boldsymbol{K}_2+\boldsymbol{K}_d\right)\boldsymbol{x}_2 - \boldsymbol{K}_p\boldsymbol{e} + \Delta\delta + \boldsymbol{u}_1 + \left(\boldsymbol{K}_2+\boldsymbol{K}_d\right)\varepsilon\boldsymbol{e} + \boldsymbol{K}_1\varepsilon\dot{\boldsymbol{e}}\right) + \frac{1}{2}\boldsymbol{x}_2{}^{\mathrm{T}}\dot{\boldsymbol{K}}_1\boldsymbol{x}_2 + \frac{1}{\alpha}\mathrm{tr}\left(\dot{\tilde{\boldsymbol{W}}}_f{}^{\mathrm{T}}\tilde{\boldsymbol{W}}_f\right)\\ &= \boldsymbol{x}_2{}^{\mathrm{T}}\left(-\left(\boldsymbol{K}_2+\boldsymbol{K}_d\right)\boldsymbol{x}_2 - \boldsymbol{K}_p\boldsymbol{e} + \boldsymbol{W}_f{}^*\boldsymbol{h}(\boldsymbol{x}) + \xi_f - \left(\boldsymbol{K}_2+\boldsymbol{K}_d\right)\varepsilon\boldsymbol{e} - \boldsymbol{K}_1\varepsilon\dot{\boldsymbol{e}} - \frac{1}{2\eta^2}\boldsymbol{x}_2\right.\\ &\quad\left. - \hat{\boldsymbol{W}}_f\boldsymbol{h}(\boldsymbol{x}) + \left(\boldsymbol{K}_2+\boldsymbol{K}_d\right)\varepsilon\boldsymbol{e} + \boldsymbol{K}_1\varepsilon\dot{\boldsymbol{e}} - \frac{1}{2}\boldsymbol{x}_2 + \boldsymbol{K}_p\boldsymbol{e}\right) + \frac{1}{\alpha}\mathrm{tr}\left(\dot{\tilde{\boldsymbol{W}}}_f{}^{\mathrm{T}}\tilde{\boldsymbol{W}}_f\right)\end{aligned} \tag{26}$$

By simplifying Eq. (26), it can be concluded:

$$\dot{V} = -\boldsymbol{x}_2{}^{\mathrm{T}}\left(\boldsymbol{K}_d+\boldsymbol{K}_2\right)\boldsymbol{x}_2 - \frac{1}{2\eta^2}\boldsymbol{x}_2{}^{\mathrm{T}}\boldsymbol{x}_2 - \frac{1}{2}\boldsymbol{x}_2{}^{\mathrm{T}}\boldsymbol{x}_2 - \boldsymbol{x}_2{}^{\mathrm{T}}\tilde{\boldsymbol{W}}_f\boldsymbol{h}(\boldsymbol{x}) + \boldsymbol{x}_2{}^{\mathrm{T}}\xi_f + \frac{1}{\alpha}\mathrm{tr}\left(\dot{\tilde{\boldsymbol{W}}}_f{}^{\mathrm{T}}\tilde{\boldsymbol{W}}_f\right) \tag{27}$$

Definition: $L = \dot{V} - \frac{1}{2}\eta^2\left|\left|\xi_f\right|\right|^2 + \frac{1}{2}||z||^2$, then,

$$\begin{aligned}L = &-\boldsymbol{x}_2{}^{\mathrm{T}}\boldsymbol{K}_d\boldsymbol{x}_2 - \boldsymbol{x}_2{}^{\mathrm{T}}\boldsymbol{K}_2\boldsymbol{x}_2 - \frac{1}{2\eta^2}\boldsymbol{x}_2{}^{\mathrm{T}}\boldsymbol{x}_2 - \boldsymbol{x}_2{}^{\mathrm{T}}\tilde{\boldsymbol{W}}_f\boldsymbol{h}(\boldsymbol{x}) + \frac{1}{\alpha}\mathrm{tr}\left(\dot{\tilde{\boldsymbol{W}}}_f{}^{\mathrm{T}}\tilde{\boldsymbol{W}}_f\right) + \boldsymbol{x}_2{}^{\mathrm{T}}\xi_f - \frac{1}{2}\eta^2\left|\left|\xi_f\right|\right|^2\\ &+ \frac{1}{2}||z||^2 - \frac{1}{2}\boldsymbol{x}_2{}^{\mathrm{T}}\boldsymbol{x}_2\end{aligned} \tag{28}$$

In Eq. (28),

$$-\boldsymbol{x}_2{}^{\mathrm{T}}\boldsymbol{K}_d\boldsymbol{x}_2 - \boldsymbol{x}_2{}^{\mathrm{T}}\boldsymbol{K}_2\boldsymbol{x}_2 \leqslant 0 \tag{29}$$

$$-\frac{1}{2\eta^2}\boldsymbol{x}_2{}^{\mathrm{T}}\boldsymbol{x}_2 + \boldsymbol{x}_2{}^{\mathrm{T}}\xi_f - \frac{1}{2}\eta^2\left|\left|\xi_f\right|\right|^2 = -\frac{1}{2}\left|\left|\frac{1}{\eta}\boldsymbol{x}_2{}^{\mathrm{T}} - \eta\xi_f\right|\right|^2 \leqslant 0 \tag{30}$$

$$\frac{1}{2}||z||^2 - \frac{1}{2}\boldsymbol{x}_2{}^{\mathrm{T}}\boldsymbol{x}_2 = 0 \tag{31}$$

$$\begin{aligned}&\frac{1}{\alpha}\mathrm{tr}\left(\dot{\tilde{\boldsymbol{W}}}_f{}^{\mathrm{T}}\tilde{\boldsymbol{W}}_f\right) - \boldsymbol{x}_2{}^{\mathrm{T}}\tilde{\boldsymbol{W}}_f\boldsymbol{h}(\boldsymbol{x}) = \frac{1}{\alpha}\mathrm{tr}\left(\tilde{\boldsymbol{W}}_f{}^{\mathrm{T}}\alpha\boldsymbol{x}_2\boldsymbol{h}(\boldsymbol{x})^{\mathrm{T}}\right) - \boldsymbol{x}_2{}^{\mathrm{T}}\tilde{\boldsymbol{W}}_f\boldsymbol{h}(\boldsymbol{x})\\ &= \mathrm{tr}\left(\tilde{\boldsymbol{W}}_f^{\mathrm{T}}\boldsymbol{x}_2\boldsymbol{h}(\boldsymbol{x})^{\mathrm{T}}\right) - \boldsymbol{x}_2{}^{\mathrm{T}}\tilde{\boldsymbol{W}}_f\boldsymbol{h}(\boldsymbol{x}) = 0\end{aligned} \tag{32}$$

Based on the above conditions, $L \leqslant 0$ can be obtained. According to the definition of L, $\dot{V} - \frac{1}{2}\eta^2\left|\left|\xi_f\right|\right|^2 + \frac{1}{2}||z||^2 \leqslant 0$ can be obtained, that is, $\dot{V} \leqslant 0$.

Therefore, based on the HJI theorem, $J \leqslant \eta$ can be obtained, so that $||z||$ satisfies the performance index, $\boldsymbol{e}$ and $\dot{\boldsymbol{e}}$ satisfy the convergence requirements.

6. Simulation analysis and results

6.1. Motion trajectory planning

When WWRTPR carries out lumbar rehabilitation training for the patients, it makes the patient's waist perform rotational rehabilitation training around the three coordinate axis (X axis, Y axis, Z axis) in the effective range according to the different degree of lumbar disease, that is, back and forth swing, left and right swing and rotation. Based on the principle of motion equivalence, the human lumbar joint is simplified as a ball hinge, and the human body is simplified as two elliptical columns connected by the ball hinge, as shown in Fig. 6.

https://doi.org/10.1017/S0263574722000376 Published online by Cambridge University Press

Table I. *Coordinates of P_i point and B_i point.*

Symbol	Coordinate point (mm)	Symbol	Coordinate point (mm)
P_1	$(-300, 191, -19.1)^T$	B_1	$(-547, 749, -1200)^T$
P_2	$(300, -190, -19.1)^T$	B_2	$(545, 749, -1200)^T$
P_3	$(300, -189, -19.1)^T$	B_3	$(549, -751, -1200)^T$
P_4	$(-300, 191, -19.1)^T$	B_4	$(-547, -751, -1200)^T$

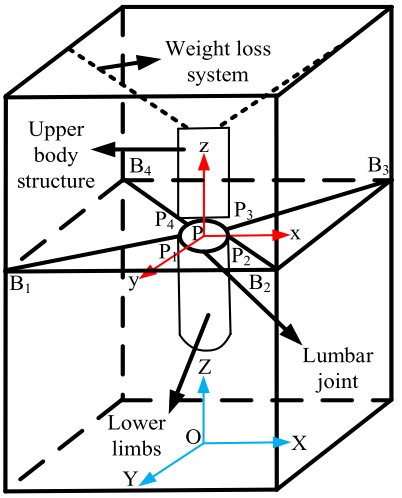

Figure 6. *Simplified schematic diagram of WWRTPR.*

In rehabilitation training, the planning of lumbar rehabilitation motion trajectory plays an important role. Unreasonable motion trajectory will cause theoretical conflict between the length and force of the wire, which will cause secondary injury to the patients. Therefore, the rehabilitation motion trajectory is reasonably planned, and the rehabilitation motion trajectory of the wire-driven lumbar rehabilitation training robot is defined as follows:

$$\begin{cases} \theta = 15^\circ \sin\left(\frac{\Pi}{10}t + \Pi\right) \\ \phi = 15^\circ \sin\left(\frac{\Pi}{10}t + \Pi\right) \\ \psi = 7^\circ \sin\left(\frac{\Pi}{10}t + \Pi\right) \end{cases} \tag{33}$$

where θ, ϕ, ψ are the rotation angles around the y-axis, x-axis and z-axis, respectively.

6.2. Simulation analysis

In order to verify the correctness and effectiveness of the designed control strategy, the force/position hybrid control strategy-based RBF neural network is simulated and analyzed for the four-wire three-degree-of-freedom wire-driven parallel robot for rehabilitation training. The simulation analysis in this section is based on the 2.5:1 scale model, and the simulation is carried out by MATLAB software. The coordinates of connection point P_i of the end effector (patient) and pulley hinge point B_i are shown in Table I, and the coordinates of P_i point and B_i point are basically symmetrically distributed.

The composite motion simulation results of lumbar rehabilitation training are shown in Figs. 7–13.

Figures 7 and 8 are, respectively, the angle trajectory curve and angle error curve of lumbar compound motion. From Fig. 7, it can be concluded that the curve of the angle trajectory of the lumbar compound movement is smooth and continuous, the angle trajectory is 0 in the median, and it reaches the expected

https://doi.org/10.1017/S0263574722000376 Published online by Cambridge University Press

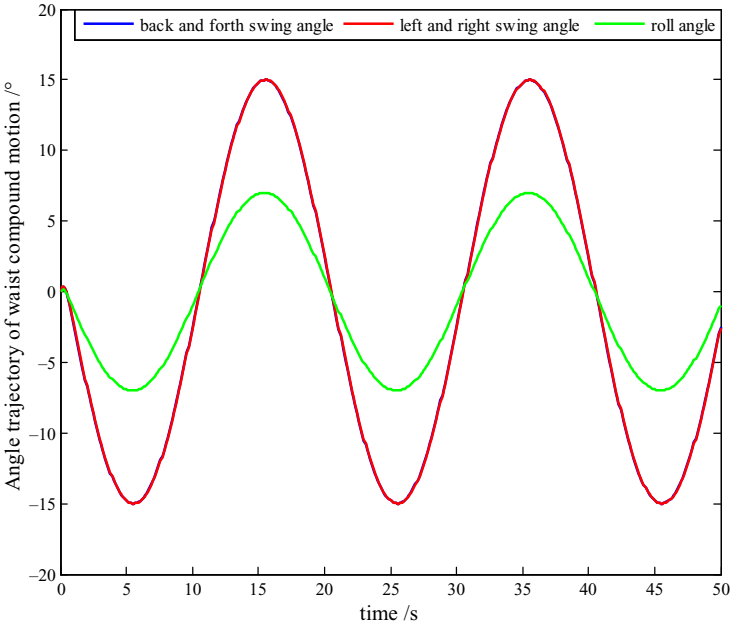

Figure 7. *Angle trajectory curve of waist compound movement.*

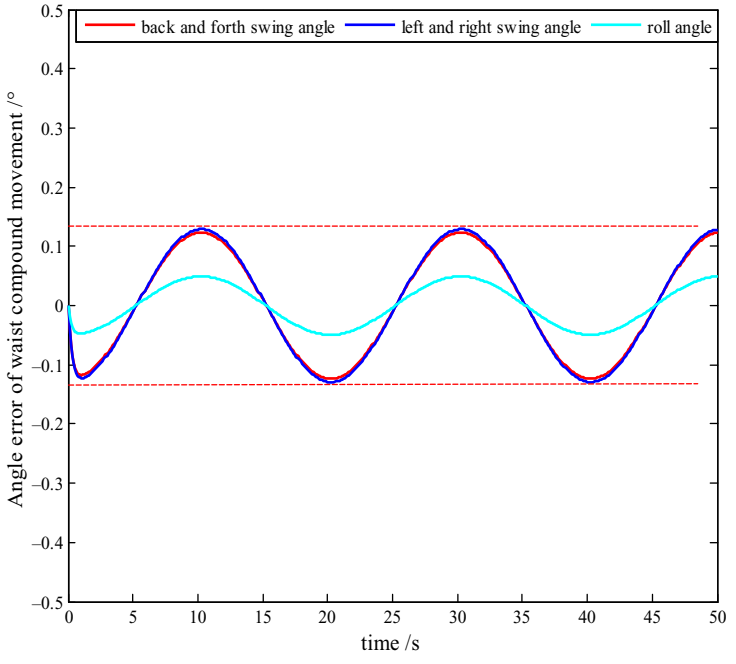

Figure 8. *Angle error curve of waist compound movement.*

limit rehabilitation value in the anterior and posterior position. From Fig. 8, it can be concluded that the angle error is within ± 0.13°, the error is small and changes within a certain range, meeting the conditions of waist compound motion.

Figures 9 and 10 are, respectively, the expected motor angular speed curve and the motor speed error curve. It can be concluded from Fig. 9 that the expected angular velocity curve of the motor is smooth

https://doi.org/10.1017/S0263574722000376 Published online by Cambridge University Press

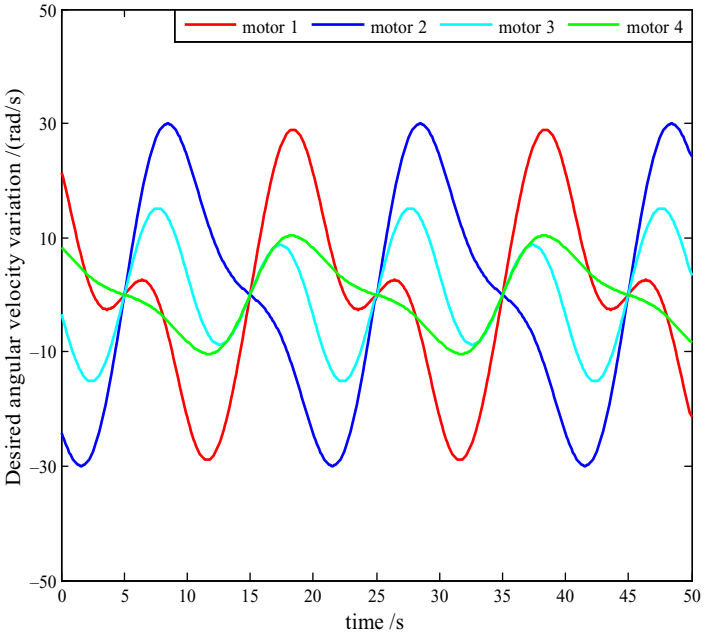

Figure 9. *Motor desired angular speed of waist compound movement.*

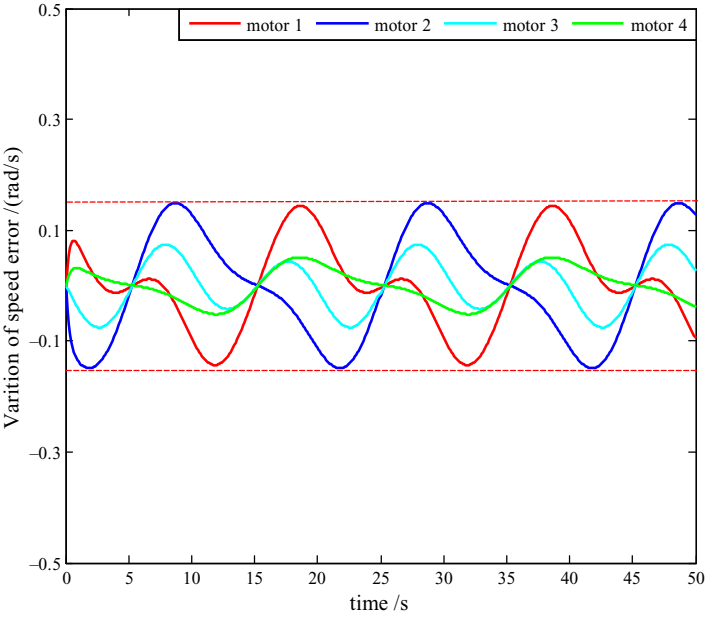

Figure 10. *Error variation of motor speed.*

and continuous, and has certain regularity. From Fig. 10, it can be concluded that the motor speed error is within ± 0.15 rad/s, and the error changes within a certain range, which meets the basic conditions of waist compound motion simulation.

Figures 11, 12 and 13 are, respectively, the wire length variation curve, wire tension variation curve and control input curve. It can be concluded from Fig. 11 that the wire length variation curve is smooth and continuous, which is similar to the trigonometric function variation, and the wire length variation

https://doi.org/10.1017/S0263574722000376 Published online by Cambridge University Press

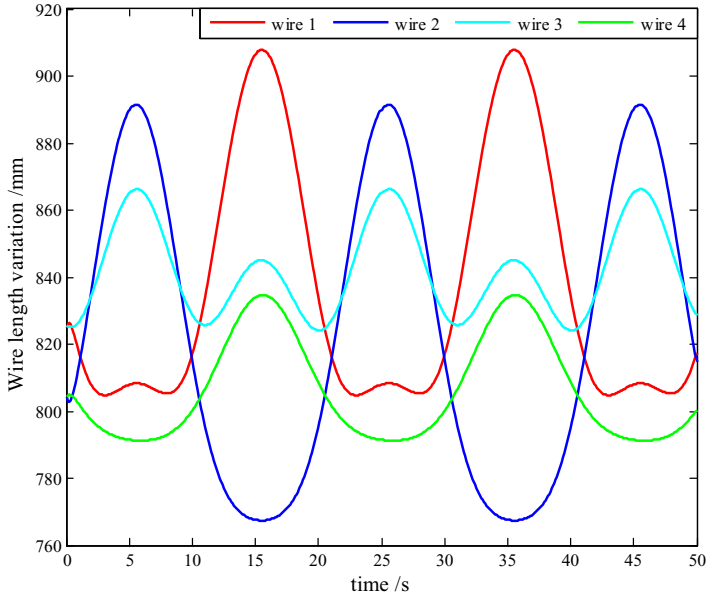

Figure 11. *Variation curve of wire length.*

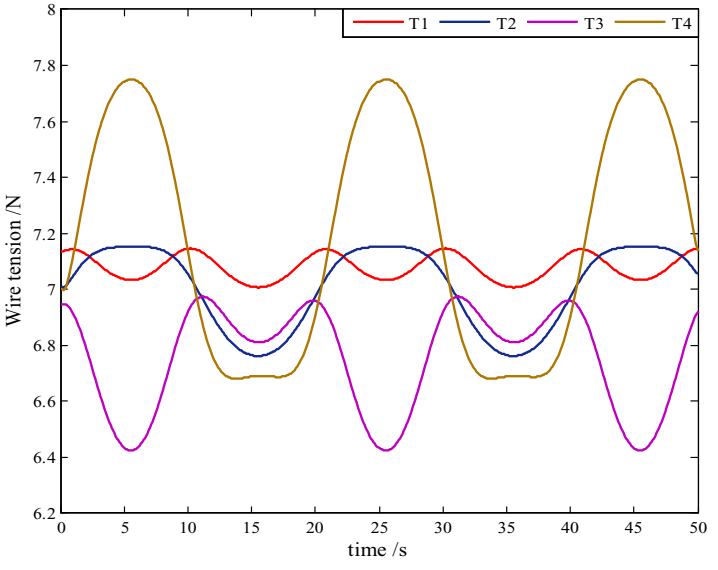

Figure 12. *Variation curve of wire tension.*

is within a certain range and has certain regularity. It can be seen from Fig. 12 that the wire tension variation is also within a certain range, and the variation is gentle, which can reduce the risk of wire interruption during rehabilitation training. It can be seen from Fig. 13 that the control input varies within the rated torque range of the motor (1.27 N. M), which conforms to the physical meaning of the design.

In conclusion, the simulation results verify the correctness, feasibility and effectiveness of the designed control strategy, and the simulation results show that WWRTPR can achieve the rehabilitation training of patients' waist, and has a certain effect on patients' waist rehabilitation.

https://doi.org/10.1017/S0263574722000376 Published online by Cambridge University Press

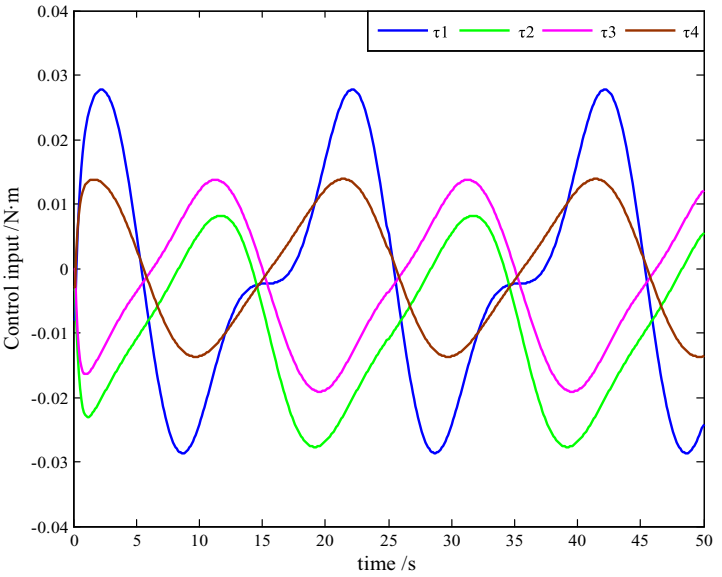

Figure 13. *Control input curve.*

7. Conclusions

In order to meet the rehabilitation training needs of patients with lumbar injury, a new type of wire-driven lumbar rehabilitation training parallel robot is designed, and an intelligent control method of force/position hybrid control based on RBF neural network is proposed, the relevant conclusions are summarized as follows:

1. According to the three-dimensional six-degree-of-freedom motion of the lumbar spine of human body, the 3D model of WWRTPR is designed and constructed. Each component of the robot system is described in detail, and the working process and working principle of each part are explained.
2. Based on the motion trajectory planning of lumbar rehabilitation training, the kinematics modeling and dynamics modeling of the robot system are analyzed, which lays the foundation for the design of the control law.
3. According to the particularity of rehabilitation training object, considering the force and pose of that patients must bear in the process of rehabilitation training, an intelligent control method of force/position hybrid control based on RBF neural network is proposed, and the stability is analyzed.
4. The motion trajectory of lumbar rehabilitation training is planned and the simulation analysis of WWRTPR is carried out. The simulation results show that WWRTPR can realize the rehabilitation training of lumbar patients, and has a certain good effect on lumbar rehabilitation.
5. In the next research, a prototype experimental platform is built to further verify the designed system and control method, test various performance parameters, and optimize the control method.

Acknowledgments. This work is supported by the Scientific Research Foundation of Nanjing Institute of Technology under Grant YKJ201917 and Natural Science Foundation of Jiangsu Province (Grant No. BK20191018).

Conflicts of interest. The authors declare that they have no conflicts of interest.

https://doi.org/10.1017/S0263574722000376 Published online by Cambridge University Press

References

[1] B. Zhang, F. Zhang, F. Zhou, W. Shang and S. Cong, "Dual-space adaptive synchronization control of cable-driven parallel robots," *Robot* **42**(2), 139–147 (2020).

[2] H. You, W. Shang, B. Zhang, F. Zhang and S. Cong, "Trajectory tracking control of cable-driven parallel robots by using high-speed vision," *J. Mech. Eng*. **55**(5), 19–26 (2019).

[3] Y. Zou, N. Wang, K. Liu and X. Geng, "Design and analysis of movable cable-driven lower limb rehabilitation robot," *J. Huazhong Univ. Sci. Technol*. **47**(1), 22–26, 38 (2019).

[4] C. Daniele, R. Matteo and C. Giuseppe, "Cube, a cable-driven device for limb rehabilitation," *J. Bionic Eng*. **16**(3), 493–503 (2019).

[5] X. Huang, H. Yu, J. Wang, Q. Dong, L. Zhang, Q. Meng, S. Li and D. Wang, "Study on the center-driven multiple degrees of freedom upper limb rehabilitation training robot," *J. Biomed. Eng* **35**(3), 452–459 (2018).

[6] Q. Chen, B. Zi, Z. Sun, N. Wang, S. Li and X. Luo, "Design, analysis and experimental study of a cable-driven parallel waist rehabilitation robot," *J. Mech. Eng*. **54**(13), 126–134 (2018).

[7] S. Gharatappeh, G. Abbasnejad, J. Yoon and H. Lee, "Control of Cable-Driven Parallel Robot for Gait Rehabilitation, The 12th International Conference on Ubiquitous Robots and Ambient Intelligence pp. 377–381.

[8] H. J. Asl and J. Yoon, "Stable assist-as-needed controller design for a planar cable-driven robotic system," *Int. J. Control Autom. Syst*. **15**(6), 2871–2882 (2017).

[9] Y. Zou, N. Wang, X. Wang, H. Ma and K. Liu, "Design and experimental research of movable cable-driven lower limb rehabilitation robot," *IEEE Access* **7**, 2315–2326 (2019).

[10] G. Aguirre-Ollinger, A. Narayan and H. Yu, "Phase-synchronized assistive torque control for the correction of kinematic anomalies in the gait cycle," *IEEE Trans. Neural. Syst. Rehabilitation Eng*. **27**(11), 2305–2314 (2019).

[11] X. Li, Q. Yang and R. Song, "Performance-based hybrid control of a cable-driven upper-limb rehabilitation robot," *IEEE Trans. Biomed. Eng*. **68**(4), 1351–1359 (2021).

[12] C. Jarrett and A. J. McDaid, "Robust control of a cable-driven soft exoskeleton joint for intrinsic human-robot interaction," *IEEE Trans. Neural Syst. Rehabilitation Eng*. **25**(7), 976–986 (2017).

[13] Q. Chen, B. Zi, Z. Sun, Y. Li and Q. Xu, "Design and development of a new cable-driven parallel robot for waist rehabilitation," *IEEE/ASME Trans. Mechatron*. **24**(4), 1497–1507 (2019).

[14] B. Zi, G. Yin and D. Zhang, "Design and optimization of a hybrid-driven waist rehabilitation robot," *Sensors* **16**(12), 2–15 (2016).

[15] V. Vashista, M. Khan and S. K. Agrawal, "A novel approach to apply gait synchronized external forces on the pelvis using A-Tpad to reduce walking effort," *IEEE Robot. Autom. Lett*. **1**(2), 1118–1124 (2016).

[16] S. Qian, B. Zi and H. Ding, "Dynamics and trajectory tracking control of cooperative multiple mobile cranes," *Nonlinear Dyn*. **83**(1-2), 89–108 (2016).

[17] Z. Gao, X. Wang, J. Wu and Q. Lin, "Hybrid force/pose control of wire-driven parallel suspension system based on stiffness optimization," *Acta Aeronautica et Astronautica Sinica* **42**, 1–12 (2021).

[18] J. P. Jun, X. Jin, A. Pott, S. Park, J.-O. Park and S. Y. Ko, "Hybrid position/force control using an admittance control scheme in Cartesian space for a 3-Dof planar cable-driven parallel robot," *Int. J. Control Autom. Syst.* **14**(4), 1106–1113 (2016).

[19] W. Shang, B. Zhang, B. Zhang, F. Zhang and S. Cong, "Synchronization control in the cable space for cable-driven parallel robots," *IEEE Trans. Ind. Electron.* **66**(6), 4544–4554 (2019).

[20] J. He. *Dynamic Modeling and Control of the Cable-Driven Parallel Robots* (Civil Aviation University of China, Tianjin, 2020).

[21] M. Shoaib, E. Asadi, J. Cheong and A. Bab-Hadiashar, "Cable driven rehabilitation robots: Comparison of applications and control strategies," *IEEE Access* **9**, 110396–110420 (2021).

[22] W. Ni, H. Li, Z. Jiang, B. Zhang and Q. Huang, "Motion and force control method of 7-Dof cable-driven rehabilitation exoskeleton robot," *Assembly Autom.* **38**(5), 595–605 (2018).

[23] Y. Wang, K. Wang, Z. Zhang and Z. Mo, "Control strategy and experimental research of a cable-driven lower limb rehabilitation robot," *Proc. Inst. Mech. Eng. C-J. Mech. Eng. Sci.* **235**(13), 2468–2481 (2021).

[24] X. Li, Q. Yang and R. Song, "Performance-based hybrid control of a cable-driven upper-limb rehabilitation robot," *IEEE Trans. Biomed. Eng.* **68**(4), 1351–1359 (2021).

[25] J. Liu. *RBF Neural Network Control for Mechanical Systems: Design, Analysis and Matlab Simulation*. 2nd edition, Tsinghua University Press, Beijing, 2018) pp. 140–142.

[26] Y. Wang, W. Sun, Y. Xiang and S. Miao, "Neural network-based robust tracking control for robots," *Intell. Autom. Soft Comput.* **15**(2), 211–222 (2009).

[27] Y. Wang, K. Wang, W. Wang, Z. Han and Z. Zhang, "Appraisement and analysis of dynamical stability of under-constrained cable-driven lower-limb rehabilitation training robot," *Robotica* **39**(6), 1023–1036 (2021).

[28] V. Bahrami, A. Kalhor and M. T. Masouleh, "Dynamic model estimating and designing controller for the 2-DoF planar robot in interaction with cable-driven robot based on adaptive neural network," *J. Intell. Fuzzy Syst.* **41**(1), 1261–1280 (2021).

[29] Z. Zake, F. Chaumette, N. Pedemonte and S. Caro, "Robust 21/2D visual servoing of a cable-driven parallel robot thanks to trajectory tracking," *IEEE Robot. Autom. Lett*. **5**(2), 660–667 (2020).

[30] Y. Lou, H. Lin, P. Quan, D. Wei and S. Di, "Robust adaptive control of fully constrained cable-driven serial manipulator with multi-segment cables using cable tension sensor measurements," *Sensors* **21**(5), 1–31 (2021).

Cite this article: W. Yuqi, C. Jinjiang, G. Ranran, Z. Lei and W. Lei (2022). "Study on the design and control method of a wire-driven waist rehabilitation training parallel robot", Robotica **40**, 3499–3513. https://doi.org/10.1017/S0263574722000376